SAIC

An Employee-Owned Company

Pacifica Technology

(2)

SAIC-90/7032

YIELD DETERMINATION UNCERTAINTIES USING THE STRONG-SHOCK ALGORITHM

M. J. Pound
and
G. I. Kent

SAIC/Pacifica Technology Division
11696 Sorrento Valley Road
San Diego, CA 92121

26 March 1990

50272-101

REPORT DOCUMENTATION PAGE	1. REPORT NO.	2.	3. Recipient's Accession No.

4. Title and Subtitle
Yield Determination Uncertainties Using the Strong-Shock Algorithim

5. Report Date
March 26, 1990

6.

7. Author(s)
M.J. Pound and G.I. Kent

8. Performing Organization Rept. No.
SAIC - 90/7032

9. Performing Organization Name and Address
Science Applications International Corporation
Pacific Division
11696 Sorrento Valley Road, Suite A
San Diego, CA 92121

10. Project/Task/Work Unit No.

11. Contract(C) or Grant(G) No.
(C) AC86VC104 Task 89-24
(G)

12. Sponsoring Organization Name and Address
Arms Control & Disarmament Agency
320 21st Street, NW
Washington, DC 20451

13. Type of Report & Period Covered
Final

14.

15. Supplementary Notes

16. Abstract (Limit: 200 words)
Data from forty explosions were reduced by the CORRTEX algorithmic method to give a yield and the resultant error of measurement. The yield uncertainty turned out to be roughly 26% for yields over 40kt. In the course of this analysis the constraints for the algorithmic equation were rederived. The yield uncertainities for tests below 50kt was postulated. The uncertainty went up considerably if the cable was close enough to be affected by ENP. For example the uncertainty, using the best methodology, was 33% at 10kt, 37% at 5kt, 46% at 2kt, and 57% at 1 kt.

17. Document Analysis a. Descriptors
Hydrodynamics
Nuclear Explosions

b. Identifiers/Open-Ended Terms
Yield Determination
Underground Test
CORRTEX

c. COSATI Field/Group Nuclear Weapons

18. Availability Statement:	19. Security Class (This Report)	21. No. of Pages
Upon Request	Unclassified	32
	20. Security Class (This Page)	22. Price
	Unclassified	

(See ANSI-Z39.18) *See Instructions on Reverse*

OPTIONAL FORM 272 (4-77)
(Formerly NTIS-35)
Department of Commerce

SAIC-90/7032

Yield Determination Uncertainties Using the Strong-shock Algorithm

M. J. Pound

G. I. Kent

SAIC, Pacifica Technology Division, San Diego, CA

26 March 1990

Abstract

We estimate the uncertainty associated with the application of the stong-shock methodology for nuclear yield determination for the idealized case of a fully-coupled event and a spherically symmetric wave field. Time-of-arrival data from a number of U. S. nuclear tests are analyzed in order to estimate measurement uncertainties and uncertainties in the algorithmic parameters. These findings are then employed to estimate resulting confidence limits for yield determinations produced via this algorithm.

1 Introduction

1.1 Background

The hydrodynamic yield algorithm is often used to estimate yields for underground nuclear events. For this algorithm, it is assumed that, under certain conditions, the yield of an underground nuclear explosion can be reasonably well determined from measurements of the propagation of the explosion-produced shock wave through the ambient geological medium. If the explosion is spherically symmetric and the measurements are taken in a pressure regime which far exceeds the yield strength of the medium (the so-called hydrodynamic regime), the shock radius appears to grow as a power-law function of time. In particular, for some range of t, the position of the shock front is assumed to be given by the generalized Taylor blast-wave solution:[1]

$$\frac{R_s}{W^{1/3}} = a\left(\frac{t}{W^{1/3}}\right)^b, \tag{1}$$

where t is time after explosion, R_s is the distance from the center of the explosion, and W is the yield of the device. The parameters a and b have been empirically determined and are assumed to be independent of the material medium and device yield over a wide range of geologic media and yields.

[1]The original derivation by Taylor,[13] for shock waves propagating in air, gave $b = \frac{2}{5}$, since he assumed a gamma-law gas with constant γ. For shocks in non-ideal materials such as rock a more general form is required.

This equation has formed the basis of the hydrodynamic-yield determination techniques used on U.S. nuclear events since the early 1960's.

We have analyzed shock time-of-arrival (TOA) data from 43 U. S. nuclear events with yields greater than 40 kt, detonated in a number of different media. Some of the questions which we have attempted to address in this analysis are: 1) Can we reliably estimate the yield of a nuclear event from TOA data alone, using the "standard" hydrodynamic yield algorithm based on Eqn. (1)? 2) If so, what are the confidence limits which can be placed on such yield estimates and how do these limits scale with variations in yield? 3) Are there any significant variations in these results for different working point media (e.g., basalt, tuff. granite)?

In this analysis we have, for simplicity, assumed that the geometry is spherically symmetric and that the events are fully coupled. For relatively large yields in reasonably small zero-room volumes, these are evidently good assumptions. As the explosive yield becomes small or as the cavity size becomes large, nonspherical effects or decoupling may become important.

1.2 The strong-shock algorithm

Here we present a brief description of the hydrodynamic or strong-shock yield algorithm as it is presently applied.[8] Figure 1 shows an example of

a typical (R_s, t) data set from a U. S. nuclear event, obtained in this case using the SLIFER[9] measurement technique. The data are presented in

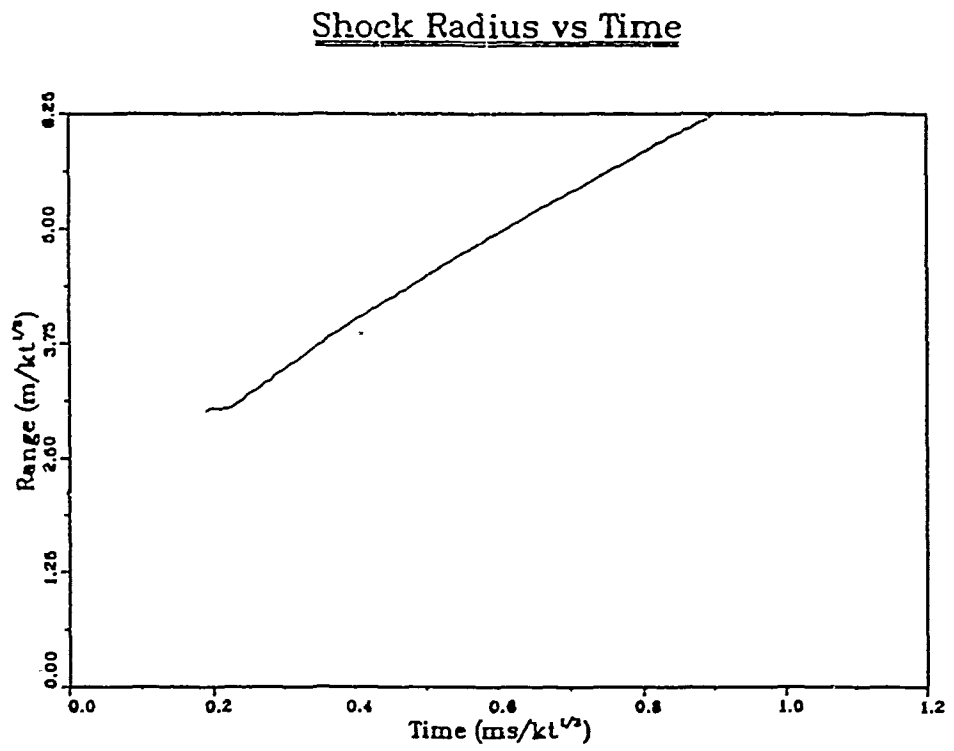

Figure 1: Scaled shock radius vs scaled time data for a typical nuclear event.

scaled form where the scaling factor for both R_s and t is the cube root of the official yield for the event, but the details of the algorithm are largely unaffected by this scaling. The most difficult part of the algorithm is making a proper determination of the region of data to analyze. Equation (1) can

be rearranged to give an explicit expression for the algorithmic yield:

$$W = \left(\frac{R_s}{at^b}\right)^{3/(1-b)} . \quad (2)$$

With this equation, given a, b, and a data set such as that shown in Figure 1, obtained from CORRTEX,[4] SLIFER, or another time of arrival measurement technique, one can reformulate the data as algorithmic yield vs time, as is shown plotted in Figure 2. Again, the quantities are scaled appropriately using the official yield for the event. There is an extremely steep region of the curve before about 0.23 scaled ms, followed by a relatively flat region between 0.23 and 0.45 scaled ms, which is in turn followed by an almost linear rise in W out to about 1 scaled ms. The very steep portion of the curve before 0.23 scaled ms is not valid data. This data is probably due to energy flow along channels near the gauge cable, causing a shock wave which arrives considerably earlier than the expected free-field shock and which is of sufficient magnitude to crush the cable. This feature is common in records from cables located in or near the device emplacement hole. The rising portion of the curve above 0.45 scaled ms is beyond the range of applicability of the algorithm owing to the increasing dominance of medium strength effects at the lower shock stress levels. Only the "flat" region of the data from 0.23 to 0.45 scaled ms is used in the determination

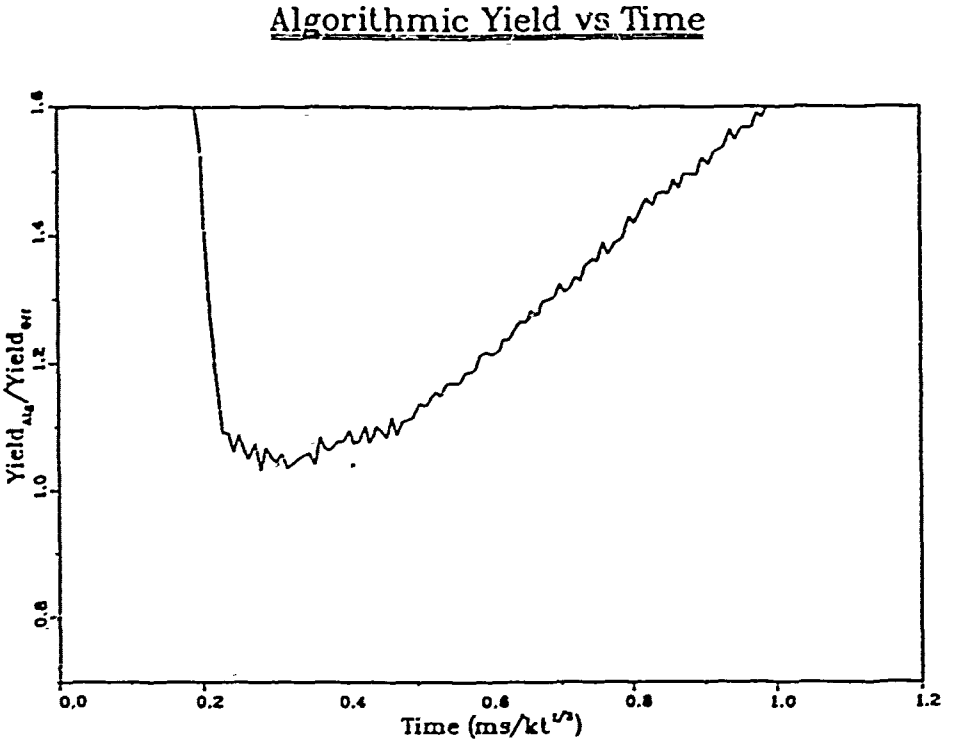

Figure 2: The ratio of algorithmic yield to official yield vs scaled time for the same event.

of the hydrodynamic yield, W_{alg}. The yield is computed by arithmetically averaging over the approximately constant values obtained from the (R_s, t) pairs within the algorithmic region,[6] although least squares fitting over the interval has been tried as well[8] with negligible change in the results obtained.

The method described here leaves room for a certain amount of inter-

pretation by the individual analyst, particularly in the determination of the time interval over which to apply the appropriate averaging operation. Historically, this step in the yield determination process has been done by hand, so that slight differences in computed yields could be calculated for the same event by different analysts working from the same data set. We have developed an automated procedure for choosing the so-called "algorithmic window" for a particular data set such as that shown in Figure 1 and have implemented the procedure in a computer program. The algorithmic time windows determined by this procedure for the 43 events considered in this report are very similar to those found by Eilers *et al.*[6] and the recalculated yields using these new windows are typically within 1% of the Eilers *et al* values. This new procedure does not therefore supply any advantage over the existing one in terms of giving better answers, but simply codifies the process of selecting the appropriate time window, thereby removing a measure of human judgement and variability from the yield determination process, in a manner which is consistent with current practice.

2 Analysis

Our primary task for this project was to estimate the uncertainty associated with employing the hydrodynamic yield algorithm to determine nuclear yields for underground events. For our hypothetical test we are to assume the data is obtained from CORRTEX measurements from cables emplaced in a satellite hole configuration. With properly placed satellite holes, contamination of the data by such phenomena as pipe flow should not be a problem For this analysis, we assume spherical symmetry for the outgoing shock front, and that the event is fully coupled.

In order to ascertain the overall uncertainty in the application of the algorithm, we begin by estimating the primary sources of uncertainty and their magnitudes. The algorithm is based on a very simple equation, Eqn. (2), with only two independent variables, R_s and t, and a very simple hypothesis, namely that Eqn. (2) holds for some range of t, given particular fixed values of a and b, independent of geologic material. Thus, our first task will be to obtain uncertainty estimates for the measured quantities R_s and t, and to judge the degree of generality with which the above hypothesis fits the observed data for the range of different media represented in the records available to us. These estimates will be based largely on a statistical

analysis of the (R_s, t) data in our database, as well as current information on the state of the art in drilling and surveying (for determining relative locations of gauges and the explosion center) and in timing technology. After these constituent uncertainties have been estimated, the three-point analysis method of Binninger and Wright[3.14] will be applied to obtain the resulting overall uncertainty in yield determinations produced by the strong-shock algorithm. The three-point methodology is an analysis tool which has proven useful in evaluating the effects of the individual uncertainties involved in the application of a more complicated procedure. We will also attempt to determine whether the "blackout region", which severely reduces the likelihood of getting useful shock time-of-arrival measurements in the extreme radiation environment near the device, places any significant restrictions on the utility of the strong-shock algorithm over any substantial portion of the yield domain of interest.

There are a number of factors which may reduce the effectiveness of yield determination techniques based on the strong-shock algorithm. First, the time-of-arrival (TOA) measurements must be taken in the hydrodynamic region of the blast, a region whose radius scales with yield and may therefore become prohibitively small for low-yield events. There is also a minimum stand-off distance inside which measurements are either impractical or use-

less. High neutron and gamma radiation levels close to the device may cause vaporization, melting or ionization of gauge elements. Also, in the very near-field, non-ideal effects due to finite source size (Eqns. (1) and (2) assume a point source) and finite cavity size become apparent. These are factors which even in the best of circumstances can limit the usefulness of algorithms based on Eqn. (1). Uncertainties in the relative locations of the gauges with respect to the effective center of the explosion may also influence our ability to make accurate yield determinations using this algorithm. These uncertainties may be related to limits on the absolute accuracy with which the gauges may be placed or determined (drilling and surveying), limited knowledge of the location of device, or offset of the effective center of the explosion (ECE) from the location of the original device center. It is conceivable that, under the circumstances of a verification situation, accurately determined point-of-origin and explosion-time fiducials may not be readily available. The effect of each of these elements would evidently become more pronounced for small yields. Our effort on this project has been aimed toward quantifying the effects of each of these and other factors on our ability to accurately make yield determinations from hydrodynamic shock location measurements.

We have attempted to quantify what we felt were the primary sources

of uncertainty associated with the application of the strong-shock algorithm to yield determination and treaty verification. One of the most important questions which must be asked pertains to the primary assumption of the strong shock algorithm itself. How well does Eqn. (1) fit data for hydrodynamic shock location in a wide variety of different geologic media using fixed values of a and b, and with what degree of confidence may it be applied in even the most ideal of situations? This question has been addressed elsewhere,[6,8] but our approach is from a somewhat different perspective.

The parameters a and b have both been empirically determined.[6] There are a number of considerations involved in the determination of the parameter b. It is clear that the location of the shock front and its velocity satisfy an equation like (1) at every instant for *some* pair of values a and b. It is likely that the appropriate value for b will lie somewhere between 0.4 (the ideal gas limit) and 1 (the linear wave limit), with the lower value applying near the source, and $b \rightarrow 1$ as $R \rightarrow \infty$. Choosing a particular value for b effectively selects a portion of the shock location history corresponding to that value. It was observed[5] in numerical experiments using realistic material models that the value $b = 0.475$ is sufficiently small to select an algorithmic region which is relatively insensitive to geologic media (i.e., is within the hydrodynamic regime), and is large enough to avoid many of the perturbations due

to emplacement geometry (e.g., pipe flow or cavity effects) which may be evident in the near-source region for many tests. This value has been used to successfully determine yields for a large number of underground nuclear tests executed in a range of different geologic media.[6,8] For this analysis, we assume a fixed value of $b = 0.475$.

2.1 Nuclear shot data.

For this analysis, we have considered shock time of arrival data from 43 U. S. DOE underground nuclear tests occurring between 1962 and 1983 and published in Eilers *et al*,[6] Goldwire and Geil[8] and Bass.[2] These represent all of the close-in (hydrodynamic) shock time-of-arrival records readily available to us for use in this analysis. All of the events in our database had yields greater than forty kilotons. Most of the data were obtained using the CORRTEX experimental technique, while the remainder come from SLIFER records. In all cases, the published "official yield" was used as the actual yield for each event. For most of the events considered here, the official yields were determined primarily from radiochemical yields, increased by calculated or estimated underground enhancements. However, for some events hydrodynamic yields were considered in the official yield determination, so that an entirely independent yield measure was not available for

analysis.

We digitized the (W,t) data points from Goldwire and Geil[8] for use in this analysis. From these data, using Eqn. (1) we were able to reconstruct what we felt was a reasonable representation of the original (R,t) data sets. The range of the data for each shot to be used in our analysis of the standard yield algorithm was taken from the Eilers *et al* paper,[6] so that we would be duplicating as closely as possible the the "standard" implementation of the algorithm. This range of useful data defines, for our purposes, the so-called *algorithmic region* for each shot.

With this information, our first analysis effort was to attempt to place some uncertainty estimates on the value of the parameter a from Eqn. (1). With a set of shock radii vs. time data, Eqn. (1) may be solved by linear least squares for a_{fit}, which minimizes the sum of the squares of the deviations between the official and computed yield at each data point in the algorithmic region. Let the sum of the squares of the deviations be given by

$$\chi^2 = \sum (W_0 - W_i)^2 = \sum \left(W_0 - \left(\frac{R_i}{a t_i^b} \right)^{3/(1-b)} \right)^2 , \qquad (3)$$

then it is easy to show that

$$a_{fit} = \frac{\sum \left(R_i / t_i^b \right)^{6/(1-b)}}{W_0 \sum \left(R_i / t_i^b \right)^{3/(1-b)}} , \qquad (4)$$

where the above summations are taken over the (R_i, t_i) data pairs within

the algorithmic region for a particular shot. Using this technique, we are able to find a best value for the parameter a (in a least-square sense) for each of the 43 events, and an associated standard deviation σ_{fit}, measuring the spread in the distribution about a_{fit} of the a_i's generated by the data, where

$$\sigma_{fit}^2 = \sum \left(a_{fit} - a_i\right)^2 = \sum \left(a_{fit} - \frac{R_i W_0^{(b-1)/3}}{t_i^b}\right)^2 . \tag{5}$$

From these results, namely, a_{fit} and σ_{fit} for each shot, we may determine the best a for all of the events together by constructing the weighted average of the individual values according to:

$$\bar{a} = \frac{\sum a_n/\sigma_n}{\sum 1/\sigma_n} , \tag{6}$$

where the a_n and σ_n are now simply the a_{fit} and σ_{fit} from Eqns. (4) and (5) for each event, and the summations are now taken over the 43 shots. The weighted standard deviation σ which is to be used as our measure of the uncertainty associated with the overall parameter $\bar{a}$, is then computed from:

$$\sigma^2 = \frac{\sum (a_n - \bar{a})^2/\sigma_n}{\sum 1/\sigma_n} . \tag{7}$$

In a similar manner, we can also construct the best a and associated standard deviation for any subset of the database, such as for the shots taken in alluvium, basalt, or some other material. Some of these results are shown

Table 1: Parameter a statistics for different media.

Category	$\bar{a}$	σ	No. cases
Alluvium	6.176	0.043	3
Basalt	6.162	0.063	2
Granite	6.221	-	1
Rhyolite	6.115	0.094	8
Tuff:			
Partially Saturated	6.107	0.054	3
Saturated	6.064	0.075	25
Tuff/Rhyolite	6.143	-	1
All shots	6.085	0.082	43
Basalt and Granite	6.164	0.062	3

in Table 1. The value of $\bar{a} = 6.085$ which we obtained as the best value for all 43 events agrees well with the Eilers *et al*[6] value of $a = 6.093$. The σ associated with each $\bar{a}$ provides a measure of how well these events fit within the framework of the algorithm with fixed values of a and b.

Note that this estimate of the uncertainty in $\bar{a}$ necessarily includes a contribution due to the uncertainty in the determination of W_0, the official yield. For example, it is *conceivable* that a single value of a is in fact correct for all of these events, and that the observed scatter is due entirely to error in the official yield determination. Although this is indeed possible, the stated official yields are our best available estimates of the actual yields, and in the absence of other independent measurements, these must be regarded as the

true yields for the events in this study.

In Figure 3 the a_{fit}'s computed using Eqn. (4) are shown plotted as a function of the density of the event medium. The best linear fit in the least-squares sense to these points is also shown, suggesting a possible small systematic density dependence for the parameter a.

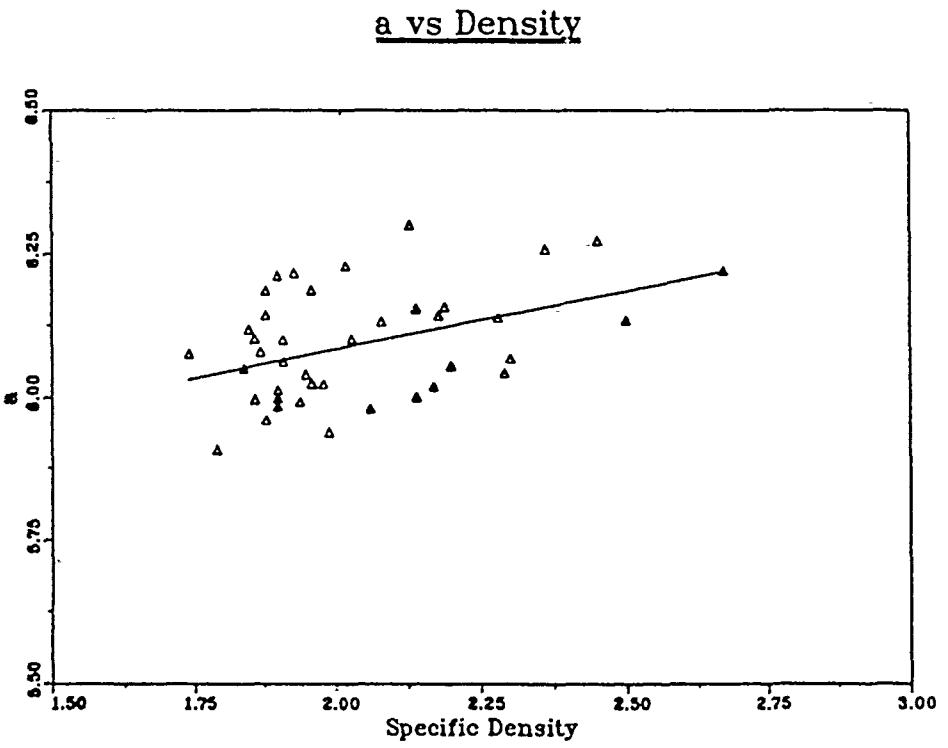

Figure 3: Parameter a plotted as a function of medium density.

A second source of uncertainty associated with application of the hydrodynamic yield algorithm stems from uncertainty in our knowledge of R_s,

the precise location of the shock front with respect to the effective center of the explosion. In this simplified analysis in which we assume that the shock is spherically symmetric, the primary causes of uncertainty in R_s are the uncertainties in the locations of particular points on the CORRTEX or SLIFER cable with respect to the device—or more properly, the effective center of explosion (ECE)—due to survey error, and uncertainty in the shock front location due to cable dynamic crush length uncertainty. Using state of the art technology, drill holes can be surveyed to accuracies of less than 0.01% of the hole depth,[11] or 1 cm at 100 meters. Dynamic crush length uncertainty, or the uncertainty associated with the exact location of the crush front on the cable, is claimed to be about ±15 cm for SLIFER and ±3 cm for CORRTEX.[6] Our analysis of the data, based on the scattering of the data points about an ideal smooth curve, suggests the overall uncertainty in R_s for all 43 events (including both SLIFER and CORRTEX records) to be about ±18.5 cm at the 2σ level. These data may reflect uncertainties in R_s due to the above factors as well as other factors not listed here, such as nonspherical shock propagation or cavity effects.

In a verification situation, limited knowledge of emplacement geometry may make it difficult to predict *a priori* the location of ECE, and accurate explosion time fiducials (to establish $t = 0$) may not be available. These

problems have been addressed in a limited sense for 1–D (spherical) geometry by Goldwire.[7] It seems clear that, in the real world of multiple dimensions, these types of *systematic* uncertainties in R_s and/or t_{os} are effectively removed by employing two or three CORRTEX cable runs routed around the device emplacement hole. Clean records from two independent measurements could be used to establish one unknown (either t_{os} or $t = 0$ if the other were known), while three independent measurements could establish both.

We estimate that the uncertainty in the measurement of t itself is negligible compared to those in a and R_s since, with modern timing devices, measurements can be made to almost arbitrary precision.

2.2 Blackout region

We also investigated the possible significance of the so-called "blackout region" inside of which TOA measurements would be precluded because of the severe radiation environment at shot time. Heat generated by the intense neutron and gamma ray fluxes close to the radiating nuclear device may lead to vaporization, melting or ionization of the TOA gauge elements, preventing valid time of arrival measurements in this region. Electromagnetic pulse (EMP) and induced Compton currents in cables and dielectrics can also

severely degrade measurements in the near-source region. We obtained estimates of the radiation fluence levels at which CORRTEX hardware could survive and successfully operate, typical n-γ fluences from a modern radiative device, and an effective absorption coefficient for γ-rays in a dense rock medium (e.g granite).[12] Ignoring any systematic dependence of the source spectrum on yield, we assume that the output fluence from the device is proportional to the yield. This leads to the equation,

$$r_B^2 e^{\mu r_B} \propto W. \tag{8}$$

where r_B is the radius of the blackout region, and the constant of proportionality may be determined from the above estimates. Carrying out this procedure, we obtain a curve for the estimated radius of the blackout region in a *dense* rock material. This curve is plotted in Figure 4. Also shown are two curves showing the approximate extent of the algorithmic window for the strong shock yield algorithm, using 0.16 ms/kt$^{1/3}$ and 0.60 ms/kt$^{1/3}$. This (estimated) inner limit of the algorithmic region lies clearly outside of the estimated blackout region, suggesting that radiation effects of this sort probably do not significantly restrict the region of validity of the strong-shock algorithm in media of this type.

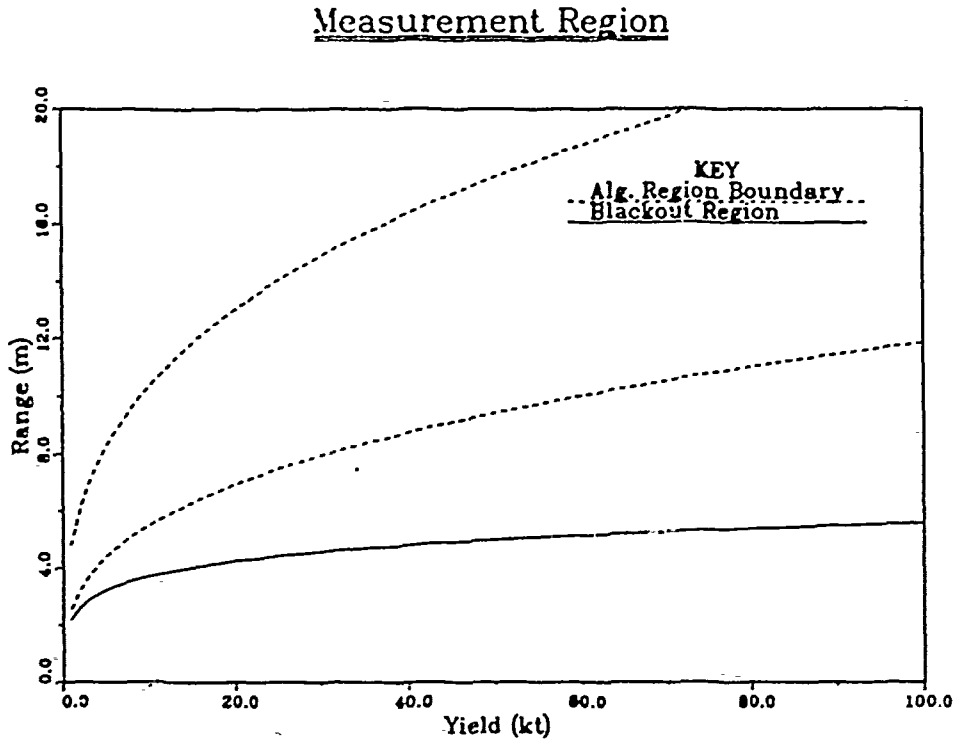

Figure 4: Blackout region and algorithmic window (estimated).

2.3 Three-point analysis

We now have identified certain error sources associated with the strong-shock yield determination methodology, and have established reasonable estimates of their constituent uncertainties. In the simplified situation considered here, the primary sources of uncertainty are believed to reside in the measurement of R, with respect to the effective center of explosion, and in the degree of universality associated with Eqn. (1) using constant values for a and b. The

next step is to assess how these constituent uncertainties affect the overall uncertainty for the yield determination method as a whole. To accomplish this, we employ the three-point analysis of Binninger and Wright. This methodology provides a quick and easy way to evaluate and rank the effects of the above uncertainties which are involved in the application of the yield algorithm. The results provided by the three-point method have been shown to compare favorably to those produced by more mathematically rigorous statistical methods such as Monte Carlo.[3]

To implement the three-point method, we first produce nominal, upper and lower bound values (at the 95% confidence level) for each of the variables which we wish to include in the uncertainty analysis. This is essentially the 2σ level for normally distributed random variables, so here we use

$$\begin{aligned} a &= \{5.921, 6.085, 6.249\} \\ R_s &= \{R_0 - 18.5\text{cm}, R_0, R_0 + 18.5\text{cm}\}\,. \end{aligned} \tag{9}$$

The value for R_0 is computed using $R_0 = at^b W^{(1-b)/3}$ with $a = 6.085$, $b = 0.475$ and $t = 0.38\ \text{ms} \times W^{1/3}$, where W is the yield in kilotons. This value for t is chosen to place it exactly in the center of the nominal algorithmic window which ranges from 0.16 to 0.60 scaled milliseconds. Clearly, R_0 is yield dependent, while a is not. For a given yield event, we now construct a table of the yields which would be predicted from a single measurement

using each combination of values in (9). As an example, for a 1 kt shot, these values would, according to Eqn. (2), generate a table of W values as shown in Table 2.

Table 2: One kiloton example.

		R_0 values			
		3.658	3.843	4.028	
a values	5.921	0.882	1.169	1.529	med = 1.169
	6.085	0.754	1.000	1.308	med = 1.000
	6.249	0.648	0.859	1.124	med = 0.859
		med = 0.754	med = 1.000	med = 1.308	

To quantify the effect of the uncertainty in a, for example, on the total dispersion in W, the variate a is fixed at its lower bound values, and then values of W are determined according to the values of R_0. These values for W are ordered according to ascending values of R_0 as shown in the first row of the matrix in Table 2. Similarly, the values of W are determined over the range of R_0 for a fixed at its nominal value (refer to the middle row), and then for a fixed at its upper value (third row).

The effect of a on the dispersion in W is then determined from the sum of the absolute differences between values in each column (measured from the median in each column). Observe that for this example the sum of absolute

differences taken over the three columns of the matrix is 0.949:

$$\begin{aligned}\mathcal{D}_a &= \sum_i \sum_j |W_{ij} - \text{med}_i| \\ &= |0.882 - 0.754| + |0.754 - 0.754| + |0.648 - 0.754| \\ &\quad + |1.169 - 1.000| + |1.000 - 1.000| + |0.859 - 1.000| \\ &\quad + |1.529 - 1.308| + |1.308 - 1.308| + |1.124 - 1.308| \\ &= 0.949 .\end{aligned} \tag{10}$$

A similar procedure is used for R_s, this time taking the absolute differences across each row. Summing these differences for each row in Table 2 we get

$$\begin{aligned}\mathcal{D}_{R_s} &= \sum_j \sum_i |W_{ij} - \text{med}_j| \\ &= 1.677 .\end{aligned} \tag{11}$$

The relative contribution of the uncertainty in a or R_s to the total dispersion in W is found by dividing the sum of the absolute differences found for each component source of uncertainty by the total sum of those calculated for both a and R_s. Thus

$$a \text{ contributes:} \quad \frac{0.949}{0.949 + 1.677} = 36\% . \tag{12}$$

and

$$R_s \text{ contributes:} \quad \frac{1.677}{0.949 + 1.677} = 64\% . \tag{13}$$

This procedure may be repeated for any desired nominal yield to generate the curves in Figure 5, which show the relative contributions of the a and R_s uncertainties as a function of yield for $0 < W \leq 150$kt.

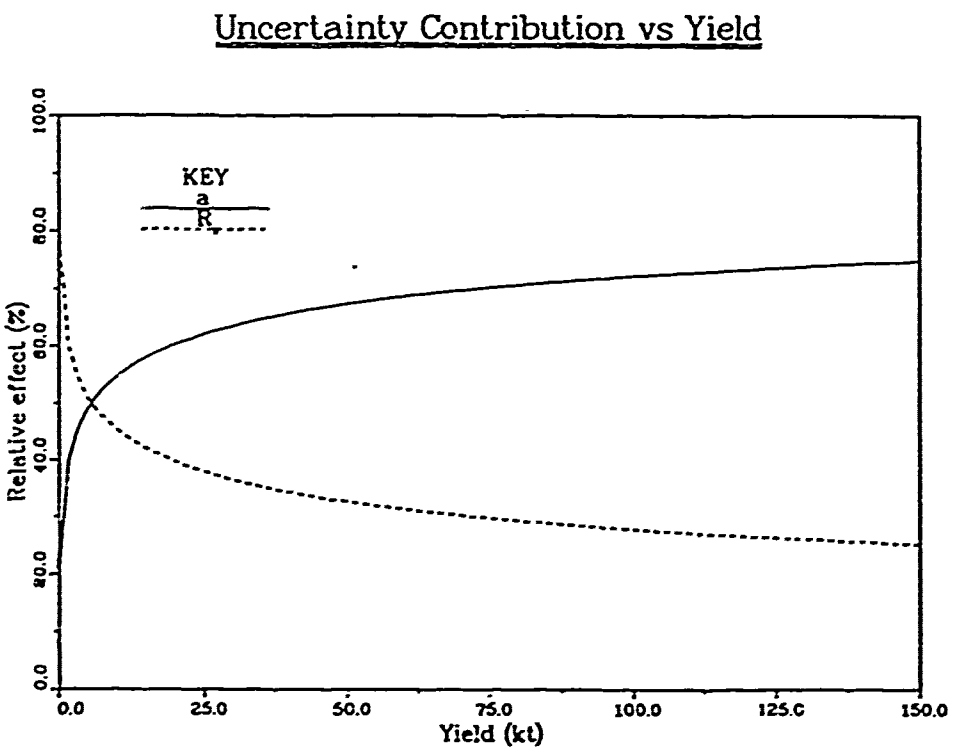

Figure 5: Relative contributions of uncertainties in a and R_s as a function of yield.

To estimate the uncertainty in yield which is produced by these sources, we use the three-point method results from Table 2 to construct the appropriate log-normal distribution corresponding to these results. The log-

normal parameters estimated from the three-point results include the median $W_{1/2}$ and β, where β is a measure of the dispersion exhibited by a log-normal variate. The log-normal distribution $f(W)$ is defined by

$$f(W) = \frac{1}{\sqrt{2\pi}\,\beta} W^{-1} \exp\{-(\ln W - \ln W_{1/2})^2/2\beta^2\}, \qquad W \geq 0. \quad (14)$$

The procedure followed to quantify these parameters is as follows:

$$\begin{aligned} W_{1/2} &= \text{median value determined from array of } W \text{ values,} \\ \beta^2 &= \frac{\sum_{ij} \left(\ln(W_{ij}/W_{1/2})\right)^2}{N-1}. \end{aligned} \quad (15)$$

For our 1 kt example, we get the log-normal parameters $W_{1/2} = 1.0$ and $\beta = 0.273$. With the distribution thus defined, we can compute the probability that W lies below a certain value, say W_F , from the equations

$$\begin{aligned} F(W_F) &= \frac{1}{\sqrt{2\pi}\,\beta} \int_0^{W_F} x^{-1} \exp\{-(\ln x - \ln W_{1/2})^2/2\beta^2\}\, dx \\ &= \frac{1}{\sqrt{2\pi}\,\beta} \int_{-\infty}^{\ln(W_F/W_{1/2})} \exp\{-x^2/2\beta^2\}\, dx \\ &= \tfrac{1}{2}\left\{1 + \operatorname{erf}\left(\frac{\ln(W_F/W_{1/2})}{\sqrt{2}\beta}\right)\right\}, \end{aligned} \quad (16)$$

where $\operatorname{erf}(z)$ is the standard *error function*.[1] Solving Eqns. (16) for $F = 95\%$, we can compute the 95% confidence level yield threshold, $W_{95\%}$, for a given yield determination. In our example, if a 1 kt yield determination were made by applying the strong-shock yield algorithm to a given set of TOA data, and assuming that the foregoing assumptions are true, then

solving Eqn. (16) with $W_{1/2} = 1$ kt and F : 95% we get $W_{95\%} = 1.57$ kt. That is, we can be 95% certain that the true yield of the measured event is below 1.57 kt. A similar procedure may be used to compute the any confidence limit, W_F, for any nominal yield $W_{1/2}$. Figure 6 shows the quantity $(W_F - W)/W$ (the fractional yield uncertainty) plotted as a function of the nominal yield, W, at the 95, 85, 75 and 65 per cent confidence levels. Each curve shows the threshold yield (at a particular level of confidence) under which we would expect a given event to fall, if the algorithmic yield had been determined as W. Thus, for example, if the algorithmic yield for a particular event is, say, 100 kt then our analysis indicates that we can be 95% confident that the true yield does not exceed this value by more than 27%. For large yields, the fractional uncertainty at the 95% confidence level appears to asymptote to about 24.5%. This is because the uncertainty in R_s becomes relatively less significant for large yields (see Figure 5), and the *yield* uncertainty becomes more dominated by the contribution from the algorithmic parameter, a, which is independent of the magnitude of the yield. As the yield approaches zero, the uncertainty in R_s becomes relatively more important and the fractional uncertainty in the determination of W increases dramatically, with fractional yield uncertainties (at 95% confidence) greater than 37% at 5 kt, 46% at 2 kt and 57% at 1 kt. For lower levels of

confidence, the fractional uncertainty curves are commensurately lower, but still show a sharp rise in the low-yield limit.

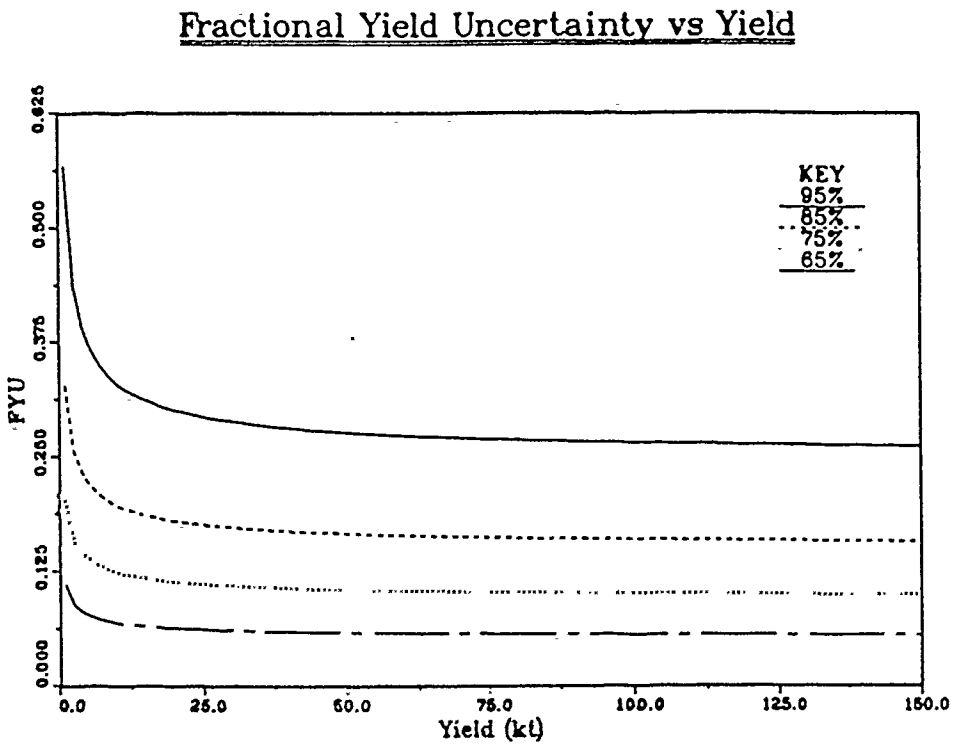

Figure 6: Fractional yield uncertainty as a function of yield.

3 Conclusions

Our finding of yield uncertainties for the strong-shock algorithm in the range of $24\frac{1}{2}$–28% for events with yields greater than about 40 kilotons is somewhat higher than the overall uncertainty of approximately 20% found by Eilers *et al*[6] and Goldwire and Geil.[8] This difference is likely attributable in large part to the differences in approach taken in the studies, and our limiting value of $24\frac{1}{2}$% for high yield is fairly close to the earlier results. These earlier studies also do not explicitly make our assumptions of a fully coupled event and spherical shock propagation. However, the ranges of yields considered effectively insured total coupling. while knowledge of the emplacement geometry, accurate time fiducials, and appropriate choice of the algorithmic time window assured that for the range of data considered the shock front was essentially spherical with known ECE. In a validation environment some of this information may not be available, so steps must be taken to assure that measurements in the hydrodynamic (algorithmic) regime are also in the region of spherical shock propagation, and a sufficient number of measurements taken to be able to pinpoint the ECE and initiation time.

We extend our results into the limit of low yields. Here we find that as the

yield goes to zero, the fractional yield uncertainty rises sharply, with yield uncertainties of about 33% at 10 kt, 37% at 5 kt, 46% at 2 kt and 57% at 1 kt. Any deleterious effects on yield analysis due to possible cavity decoupling, timing uncertainties, asymmetric device placement or other nonspherical geometry would of course be magnified at low yields, increasing the level of uncertainty in the resultant algorithmic yields in this regime.

Our analysis shows that the so-called "blackout region" in which measurements are precluded due to the extreme radiation environment does not appear to significantly restrict the application of the algorithm for events surrounded by a dense geologic medium. If a significant amount of the material between the device and the measurement regime is air (as in the case of a large emplacement cavity, for example), the range of this exclusion region would of course be extended, possibly precluding valid TOA measurements in the algorithmic region.

For fixed $b = 0.475$, the algorithmic parameter a does not show any strong systematic media dependence, although there is a slight indication of variation with material density. This finding is in general agreement with that of Goldwire and Geil.[8] Most of the data available to us were from events executed in fully saturated tuff (25 out of 43 shots), with few shots in each of six other types of geology. We believe that there is sufficient data

to establish that a does not vary much with geology, but useful conclusions about the magnitude of the variation which might be used to fine-tune the algorithm require more data in media other than tuff.

Finally, we must mention that our analysis is based upon a special data set, in particular, one in which all of the records have some valid algorithmic data. A more representative sampling of data records may include records without any valid data in the algorithmic region (due primarily to aspherical shock propagation or cavity effects). Such cases may be difficult to detect without independent knowledge of the device yields. Using satellite holes for CORRTEX reduces this risk by avoiding pipe-flow problems, but the effect may be similar for a small-yield event taking place in a relatively large cavity, since the algorithmic region is necessarily close to the cavity wall in these cases. This effect may be increased by asymmetric placement or detonation of the device. Care must be taken to apply our results in such a way that our assumptions of total coupling and spherical shock propagation are valid.

References

[1] Abramowitz, M. and I. A. Stegun, eds., *Handbook of Mathematical Functions with Formulas, Graphs, and Mathematical Tables*, National Bureau of Standards. Washington, D. C., 1964.

[2] Bass, R. C., "An experimental description of the shock front produced by a contained nuclear detonation in a granite medium", Sandia Laboratory, Albuquerque, NM, SC-RR-68-173 (1968).

[3] Binninger, G. and S. C. Wright, "Targeting uncertainties methodology", Defense Nuclear Agency Technical Report, DNA-TR-87-273-V2 (1987).

[4] Deupree, R. G., *et al*, "CORRTEX: A compact and versatile system for time domain reflectometry," Los Alamos National Laboratory, Los Alamos, NM, LA-UR-80-3382 (1981).

[5] Eilers, D. D., Los Alamos National Laboratory, Los Alamos, NM, *private communication*, January 1990.

[6] Eilers, D. D., *et al*, "A hydrodynamic yield verification algorithm applied to U. S. underground nuclear tests (U)," Los Alamos National Laboratory, Los Alamos, NM, LA-11125-MS (1987) (S-FRD).

[7] Goldwire, Jr., H. C., "Solving the strong-shock algorithm for explosive yield and spatial origin," Los Alamos Scientific Laboratory, Los Alamos, NM, LA-6786 (1977).

[8] Goldwire, Jr., H. C.. and R. G. Geil, "Empirical basis of the strong shock yield algorithm (U)," Lawrence Livermore National Laboratory, Livermore, CA, UCRL-53818 (1987) (S-FRD).

[9] Heusinkveld, M., and F. Holzer, "A method of continuous shock front position measurement," Lawrence Radiation Laboratory, Livermore, CA, UCRL-7449 (1963).

[10] King, D. S., *et al*, "The effective yield of a nuclear explosion in a small cavity in geologic material: Enhanced coupling revisited," *J. Geophys. Res.*, 94 (1989), 12375-12385.

[11] Melzer, L. S., Science Applications International Corporation, Midland, TX, *private communication*, September 1989.

[12] Sites, K. R., Science Applications International Corporation, Las Vegas, NV, *private communication*, October 1989.

[13] Taylor, G. I., "The formation of a blast wave by a very intense explosion, I. Theoretical discussion," *Proc. R. Soc. London, Ser. A*, **201** (1950), 159–174.

[14] Wright, S. C., "Damage expectancy uncertainties for deeply buried targets", Defense Nuclear Agency Technical Report, DNA–TR–89–163 (1989).